

# GOAL: Generating 4D Whole-Body Motion for Hand-Object Grasping

Omid Taheri Vasileios Choutas Michael J. Black Dimitrios Tzionas

Max Planck Institute for Intelligent Systems, Tübingen, Germany

{otaheri, vchoutas, black, dtzionas}@tue.mpg.de

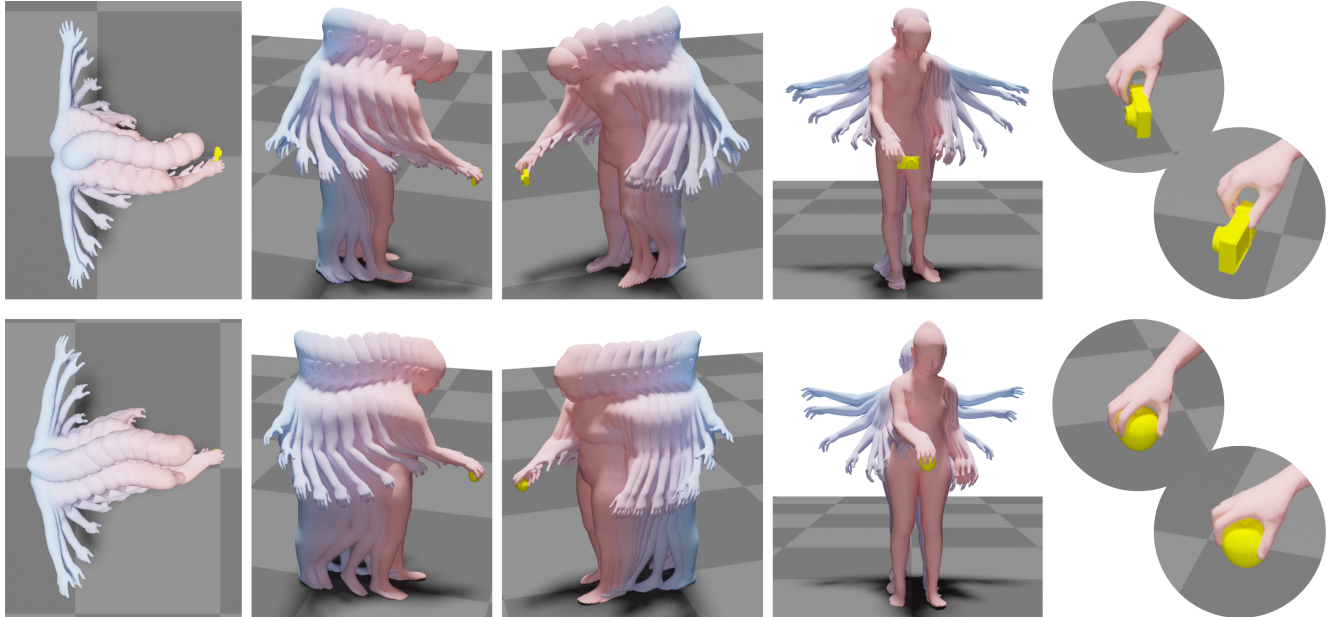


Figure 1. GOAL generates whole-body motions for approaching and grasping an unseen 3D object. The figure shows generated motions for 2 people (top, bottom), each grasping a different novel object. For each sequence we show 4 different views (left to right), as well as zoomed-in “circle” snapshots of the final grasp. GOAL is the first method to generate such a natural motion and grasp for the full body.

## Abstract

Generating digital humans that move realistically has many applications and is widely studied, but existing methods focus on the major limbs of the body, ignoring the hands and head. Hands have been separately studied but the focus has been on generating realistic static grasps of objects. To synthesize virtual characters that interact with the world, we need to generate full-body motions and realistic hand grasps simultaneously. Both sub-problems are challenging on their own and, together, the state space of poses is significantly larger; the scales of hand and body motions differ, and the whole-body posture and the hand grasp must agree, satisfy physical constraints, and be plausible. Additionally, the head is involved because the avatar must look at the object to interact with it. For the first time, we address the problem of generating full-body, hand and head motions of an avatar grasping an unknown object. As input, our method, called GOAL, takes a 3D object, its posi-

tion, and a starting 3D body pose and shape. GOAL outputs a sequence of whole-body poses using two novel networks. First, GNet generates a goal whole-body grasp with a realistic body, head, arm, and hand pose, as well as hand-object contact. Second, MNet generates the motion between the starting and goal pose. This is challenging, as it requires the avatar to walk towards the object with foot-ground contact, orient the head towards it, reach out, and grasp it with a realistic hand pose and hand-object contact. To achieve this the networks exploit a representation that combines SMPL-X body parameters and 3D vertex offsets. We train and evaluate GOAL, both qualitatively and quantitatively, on the GRAB dataset. Results show that GOAL generalizes well to unseen objects, outperforming baselines. A perceptual study shows that GOAL’s generated motions approach the realism of GRAB’s ground truth. GOAL takes a step towards synthesizing realistic full-body object grasping. Our models and code will be available at <https://goal.is.tuebingen.mpg.de>.

## 1. Introduction

Virtual humans are important for movies, games, AR/VR and the metaverse. Not only do they need to look realistic, but also move and *interact* realistically. Most work on human motion generation has focused only on bodies, without the head and hands. Often, these bodies are considered in “isolation”, with no scene or object context. Other work focuses on bodies interacting with scenes, but ignores the hands. Similarly, work on generating hand grasps often ignores the body. We argue that these are all just parts of the problem. What we really need, instead, is to generate the motion of *whole-body* avatars *grasping* objects, by jointly considering the body, head, feet, hands, as well as objects. We address this here for the first time.

The problem is challenging and multifaceted. Think of how we grasp objects in real life (see [Fig. 2](#)); we walk towards the object with our feet contacting the ground, we orient our head to look at the object, lean our torso and extend our arms to reach it, and dexterously pose our hands to establish fine contact and grasp it. Humans are able to gracefully execute these steps, yet, these are challenging and involve motion planning, motor control, and spatial awareness. Some of these steps have been studied separately, but we cannot simply combine the partial solutions since the entire action must be *coordinated*. This is challenging because: (1) full bodies have a much higher-dimensional state space than bodies or hands alone; (2) the body and hands have very different sizes, motion scales and level of dexterity; (3) the body, head and hands must move in a coordinated fashion. Currently, there are no automatic tools to generate such coordinated full-body grasping motions.

We address this with *GOAL*, which stands for *Generating Object-interActing wholE-Body motions*. GOAL generates whole-body avatar motion for grasping an unknown object, by jointly considering the body, head, feet, hands and the object. GOAL takes three *inputs*: (1) a 3D object, (2) its position and orientation, and (3) a “starting” 3D body pose and shape, positioned near the object and roughly oriented towards it. As output, GOAL generates a sequence of 3D body poses from the starting pose through to an object grasp. To do so, GOAL uses two novel networks (for an overview see [Fig. 3](#)): (1) First, GNet generates a “goal” whole-body grasp, with a realistic body pose, head pose, arm pose, and hand pose, as well as realistic finger-object and foot-ground contact. GNet is formulated as a conditional variational auto-encoder (cVAE), thus, it learns a distribution over grasping poses, and can generate a variety of “goal” grasps. (2) Then, MNet inpaints the motion between the “starting” and “goal” poses, by generating a sequence of whole-body poses in an auto-regressive fashion. This is challenging because the avatar needs to (see [Fig. 1](#)) walk by taking a number of steps proportional to the distance to the object, while having natural foot-ground contact with-

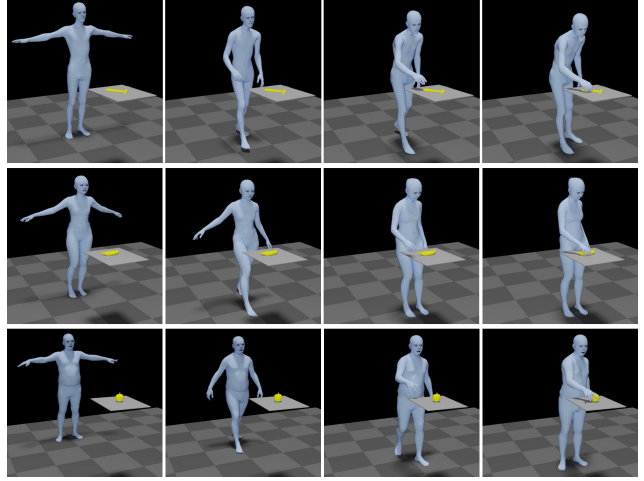


Figure 2. Grasping an object involves several motions. We walk towards the object with our feet contacting the floor, we orient our head to look at the object, we lean our torso, extend our arms, and pose our hand to contact and grasp the object. The depicted examples use motions captured in the GRAB dataset [55].

out “skating”, and continuously orient the head to look at the object. Then, when it is near the object, it needs to slow down, stop walking, lean the torso, extend the arms to reach the object. It must also pose the hand to contact the object and grasp it. All body parts need to move gracefully and in full coordination, so that the motion looks natural.

Achieving this level of realism requires technical novelties. GOAL draws inspiration by recent work [36, 62, 64], but goes beyond this to uniquely infer both SMPL-X [44] parameters and 3D offsets. GNet infers 3D hand-to-object vertex offsets to give spatial awareness and guide object grasping. MNet infers 3D SMPL-X vertex offsets to guide SMPL-X deformation from the previous to the current frame. These offsets lie in 3D Euclidean space, thus, they can be more accurately inferred than SMPL-X parameters, and are used in an offline optimization scheme to refine SMPL-X poses. We train GNet and MNet on the GRAB [55] dataset, which contains whole-body SMPL-X humans grasping objects.

We evaluate GOAL, both quantitatively and qualitatively, on withheld parts of the GRAB dataset. Specifically, we withhold 5 objects for testing. Results show that GOAL generalizes well and produces natural motions for full-body walking and object grasping; see [Fig. 1](#). Quantitative evaluation shows that GOAL outperforms baselines, and ablation studies show a positive contribution of all major components. A perceptual study verifies the above, while showing that GOAL’s generated motions achieve a level of realism comparable to GRAB’s ground-truth motions.

GOAL takes a step towards generating whole-body grasp motion for realistic avatars. Models and code will be available at <https://goal.is.tuebingen.mpg.de>.

## 2. Related Work

**Motion generation for bodies “in isolation”:** Research on human motion generation has a long history [2, 4, 59]. However, even recent methods [39, 47, 61, 64], mostly study the body “in isolation”; i.e., with no scene context. Most methods generate the motion of 3D skeletons [13, 22, 39–41, 61], while others [16, 47, 64] generate the motion of a human model like SMPL [37]. Typically, 1-2 seconds of motion synthesis is referred to as “long term”. Early deep-learning methods employ RNNs [10, 13, 42], but they struggle with discontinuities between the observed and predicted poses, as well as with long-range spatio-temporal relations. Other methods tackle these with phase-functioned feed-forward neural networks [21, 54], i.e. by conditioning network weights on phase, but they focus on cyclic motions. More recent methods [34, 39, 47, 56] use attention [57].

**Motion generation for bodies in 3D scenes:** Most early methods extend MoCap databases with point annotations for foot and hand contact [12, 25, 31, 32]. Then, they fit motion to contacts with optimization and space-time constraints for 3D body motion re-targeting [12], and animating bodies that move in 3D terrains [25, 31, 32].

To avoid big MoCap datasets, some methods use deep reinforcement learning (RL) for body-scene [5, 45, 46] or hand-object [6, 11] interactions. These methods show promising results for navigating terrains with varying height and gaps [45, 46], sitting on chairs [5, 54], using a hammer and opening a door [11], and for in-hand object re-orientation [6]. Generalization to new bodies, object geometry, and interaction types remains a challenge.

Others follow a 3D geometric approach. Pirk et al. [48] place virtual sensors on objects to sense the flow of points sampled on an agent interacting with these, and build functional object descriptors. Al-Asqhar et al. [1] re-target body motion by encoding human joints w.r.t. fixed points sampled on a scene. Ho et al. [20] use body and object vertices to compute per-frame “interaction meshes”, and minimize their Laplacian deformation to re-target body motion. These pure geometric methods are not robust to real-world noise.

In contrast, we fall in the category of data-driven methods. Corona et al. [7] generate the context-aware motion of a human skeleton interacting with objects, where “context” is encoded as a directed graph connecting person and object nodes. More relevant are methods for generating motion between a “start” and a “goal” pose in a 3D scene. Hassan et al. [17] estimate a “goal” position and interaction direction on an object, plan a 3D path from a “start” body pose to this, and finally generate a sequence of body poses with an auto-regressive cVAE for walking and interacting, e.g., sitting on a chair. Wang et al. [58] first estimate several “sub-goal” positions and bodies, divide these into short start/end pairs to synthesize short-term motions, and finally stitch these together in a long motion with an optimization process.

**Motion generation for hands:** ElKoura1 et al. [9] estimate physically plausible hand poses for playing musical instruments, using a low dimensional pose space learned from data. Pollard et al. [49] use MoCap to learn a controller for physically-based grasping. Kry et al. [30] capture hand MoCap and forces with sensors placed on objects, and use these to build “interaction trajectories” for synthesizing or re-targeting motions with physics simulation. More related to us, Lie et al. [60] take as input MoCap data of body and object motion, and add the missing hand motion to the body by first searching for feasible contact-point trajectories and then generating smooth hand motion with space-time optimization that satisfies the estimated contacts.

**Pose generation for bodies in 3D scenes:** Early methods use either contact annotations [35] or detections [27] on 3D objects, and fit 3D skeletons to these. Other methods use physics simulation to reason about contacts and sitting comfort [24, 33, 66]. Focusing on rooms instead of single objects, Grabner et al. [14] predict all areas on a 3D scene mesh where a 3D human mesh can sit, using proximity and intersection metrics. Recent methods [18, 63, 65] use deep learning to generate static humans interacting with a scene. Zhang et al. [65] learn a cVAE to generate SMPL-X [44] poses, conditioned on an input depth image and semantic segmentation of the scene. Zhang et al. [63] use an explicit scene-centric representation of interaction, while Hassan et al. [18] use a human-centric interaction representation that they embed in the SMPL-X [44] statistical body model.

**Pose generation for hand-object grasps:** Taheri et al. [55] infer MANO [53] grasps for a 3D object, by first predicting a rough grasp, and then refining it with distance and contact metrics. Grady et al. [15] first estimate contacts on both the hand and object, and then refine hand poses with optimization to satisfy contacts. Karunratanakul et al. [26] infer a “grasping” distance field and then fit MANO to it.

**Motion for full-body interactions:** People use their body and hands together for interacting with the world. Hsiao et al. [23] build a database of whole-body grasps with a human operating an avatar, and perform imitation learning. Borras et al. [3] capture whole-body MoCap data [38] of people interacting with scene objects and handheld objects using a humanoid model, and define a pose taxonomy. Taheri et al. [55] capture whole-body SMPL-X [44] interactions with handheld objects, but learn a cVAE that generates only static grasping hands, due to the task complexity. Merel et al. [43] use deep RL and human MoCap demonstrations to learn a vision-guided neural controller for picking up and carrying boxes, or catching and throwing a ball.

**Summary:** The community has focused only on parts of the problem (either the body or the hands) or used unrealistic body models. GOAL learns to generate full-body SMPL-X motion for walking towards an object up to grasping it, given only a 3D object and a “start” human pose.

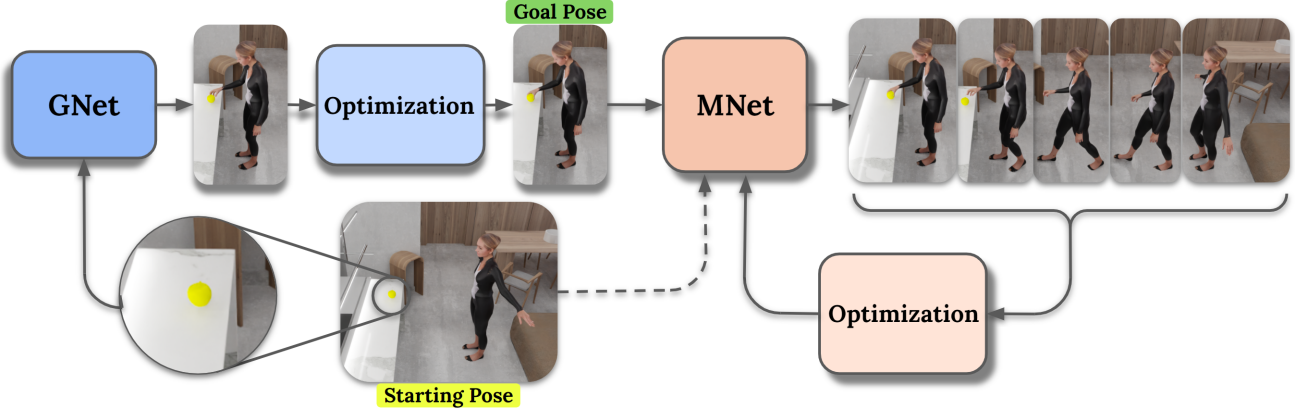


Figure 3. Overview of GOAL. There are two main stages: (1) GNet takes as input the object and its location, and generates a “goal” whole-body grasping pose. The output pose is refined with optimization post processing to look more realistic and physically plausible. (2) MNet takes as input a starting pose and the generated “goal” pose for the human, and generates the motion in between as a sequence of poses in an auto-regressive fashion. The output poses are refined with optimization post processing to better “reach” the “goal” pose.

### 3. Method

An overview of our method, GOAL, is shown in Fig. 3. GOAL takes three *inputs*, namely: (1) a 3D object, (2) its position and orientation, and (3) a “starting” 3D body pose and shape, positioned near the object (roughly 0.5 – 1.5 m) and oriented towards it (roughly  $\pm 10^\circ$ ). Then, as *output*, GOAL generates SMPL-X motion with two main networks: (1) GNet synthesizes a “goal” SMPL-X mesh that grasps the 3D object with a realistic body pose and hand-object contact; (2) MNet “inpaints” the motion from the “start” to the “goal” pose, by generating a sequence of “moving” SMPL-X bodies in an auto-regressive way. Without loss of generality, we model right-handed grasps.

#### 3.1. Human Model

We use the SMPL-X [44] statistical 3D whole-body model, which jointly captures the body, head, face and hands. SMPL-X is a differentiable function that takes as input shape,  $\beta$ , pose,  $\theta$ , and expression,  $\psi$ , parameters and then outputs a 3D mesh,  $M$ , with 10,475 vertices,  $V$ , and 20,908 triangles,  $F$ . The shape vector  $\beta \in \mathbb{R}^{20}$  contains coefficients of a low-dimensional space, created via PCA on 3D meshes of roughly 4,000 different people [52]. The vertices are posed with linear blend skinning with a learned rigged skeleton with joints  $\mathcal{J} \in \mathbb{R}^{55 \times 3}$ . Let  $\Theta = \{\theta, t\}$  be all SMPL-X parameters we predict, where  $\theta \in \mathbb{R}^{55 \times 6}$  [67],  $t \in \mathbb{R}^3$ . In the following, instead of using all SMPL-X vertices, we sample 400 vertices on body areas that are important for interactions using GRAB’s [55] contact heatmaps.

#### 3.2. Interaction-Aware Attention

Two common representations for body-object interaction are: vertex-to-vertex distances between meshes and contact

maps on meshes. However, the former carries information that is irrelevant to the interaction (e.g., vertices far away from the object), while the latter is too compact and carries no information about 3D proximity before/after contact.

Here, we use vertex-to-vertex distances, but introduce a novel “interaction-aware” attention that focuses more on body vertices that are important for interaction (e.g., hands for grasping, feet for walking) and less to irrelevant vertices (e.g., knees are less relevant than the hand for grasping). Our “interaction-aware” attention is formulated as:

$$I_w(d) = \exp(-w \times d), \quad w > 0 \quad (1)$$

where  $w$  is a scalar weight,  $d \in \mathbb{R}^D$  is a body-to-object distance vector, and  $D$  is the number of sampled vertices on SMPL-X, and is 400 for the body and 99 for the hand. This gives exponentially bigger attention to vertices relevant for interaction. The attention is visualized in Fig. 4; note that the attended body areas are meaningful. We set  $w = 5$ , which empirically results in realistic grasps and motions.

#### 3.3. “Goal” Network (GNet)

GNet is a conditional variational auto-encoder (cVAE) [29] that generates a static whole-body grasp, conditioned on the given object and its location. To do this, we first encode whole-body grasps into an embedding space.

**Input:** The input  $X$  to the encoder is:

$$X = [\Theta, \beta, v, d^{b \rightarrow o}, h, t^o, b^o] \quad (2)$$

where  $\Theta$  is the SMPL-X parameters,  $v \in \mathbb{R}^{400 \times 3}$  is the 3D coordinates of the sampled SMPL-X vertices,  $h \in \mathbb{R}^3$  is a unit vector for head orientation,  $t^o \in \mathbb{R}^3$  is the object translation and  $b^o \in \mathbb{R}^{1024}$  is the Basis Point Set (BPS) [50] representation of the 3D object shape.  $d(v^s, v^t) \in \mathbb{R}^{N \times 3}$  is

a function that computes offset vectors from the vertices of the source mesh  $\mathbf{v}^s$  to the closest vertices of the target mesh  $\mathbf{v}^t$ :  $\mathbf{d}_i(\mathbf{v}_i^s, \mathbf{v}_i^t) =$

$$I_w (\|\mathbf{v}_i^s - \mathbf{v}_k^t\|_2), k = \arg \min_j \|\mathbf{v}_i^s - \mathbf{v}_j^t\|_2. \quad (3)$$

We use this function to compute  $\mathbf{d}^{b \rightarrow o} = \mathbf{d}(\mathbf{v}, \mathbf{v}^o)$ , the offset vectors from the sampled body vertices,  $\mathbf{v}$ , to the closest object vertices,  $\mathbf{v}^o$ .

At training time, the encoder  $\mathcal{E}^G$  maps the inputs  $X$  to the parameters of a normal distribution  $\mu, \sigma \in \mathbb{R}^{16}$ . We then sample a latent whole-body grasp code  $\mathbf{z}_g \in \mathbb{R}^{16}$  from this distribution using the re-parameterization trick [29]. Note that during inference we use the 16-dimensional standard normal distribution to sample  $\mathbf{z}_g \sim \mathcal{N}(0, I)$ .

**Output:** The decoder takes the grasp code  $\mathbf{z}_g$ , the input conditions for the object,  $\mathbf{C} = [b^o, t^o]$ , and predicts SMPL-X parameters  $\Theta$ , the head direction vector  $\hat{\mathbf{h}}$ , and offset vectors  $\hat{\mathbf{d}}^h$  from 99 sampled right-hand vertices,  $\mathbf{v}_h \subset \mathbf{v}$  to object vertices.

Both the encoder and decoder use fully-connected layers with skip connections, GNet is trained end-to-end and the loss is defined as  $\mathcal{L} = \lambda_v \mathcal{L}_v +$

$$\lambda_v^h \mathcal{L}_v^h + \lambda_p \mathcal{L}_p + \lambda_h \mathcal{L}_h + \lambda_{d^h} \mathcal{L}_{d^h} + \lambda_{KL} \mathcal{L}_{KL}, \quad (4)$$

where  $\mathcal{L}_v = \|\mathbf{v} - \hat{\mathbf{v}}\|_1$ ,  $\mathcal{L}_v^h = \|\mathbf{v}^h - \hat{\mathbf{v}}^h\|_1$ ,  $\mathcal{L}_p = \|\Theta - \hat{\Theta}\|_2$ ,  $\mathcal{L}_h = \|\mathbf{h} - \hat{\mathbf{h}}\|_2$ ,  $\mathcal{L}_{d^h} = \|\mathbf{d}^h - \hat{\mathbf{d}}^h\|_1$ , and  $\mathcal{L}_{KL}$  denotes the Kullback-Leibler divergence. The hat denotes regressed quantities; the non-hat variables are ground truth. For the exact architecture of GNet, see [Appx.](#).

We make two empirical observations: (1) Networks struggle to predict accurate SMPL-X parameters, possibly due to their non-Euclidean space. (2) Networks predict interaction features in a Euclidean space much more precisely. These observations are in line with recent work [36, 62, 64], but we go beyond them in regressing 3D *offsets* together with SMPL-X parameters, instead of regressing point positions and fitting SMPL-X to these. We leverage offsets in an optimization step to refine our SMPL-X predictions.

**GNet Optimization:** We leverage the predicted offsets to refine our SMPL-X predictions with optimization post processing. Specifically, we *optimize* over SMPL-X pose,  $\theta$ , and translation,  $t$ , initialized with GNet’s predictions. Instead of hand-crafted contact constraints [8, 19, 58] during optimization, we use data-driven constraints *generated* from GNet. Specifically, we use: (1) hand-to-object vertex offsets, (2) head-orientation and (3) pose coupling to the initial value, and (4) foot-ground penetration.

In technical terms, for refining the hands to realistically grasp the objects, we define a  $l_1$  term between the offsets  $\hat{\mathbf{d}}^h$  generated from the GNet, and offsets computed online from SMPL-X’s hand vertices to the closest object vertices:

$$\mathbf{E}_d(\theta; t; \hat{\mathbf{d}}^h) = \|\mathbf{d}(\mathbf{v}^h(\theta; t, \mathbf{v}^o) - \hat{\mathbf{d}}^h\|_1. \quad (5)$$

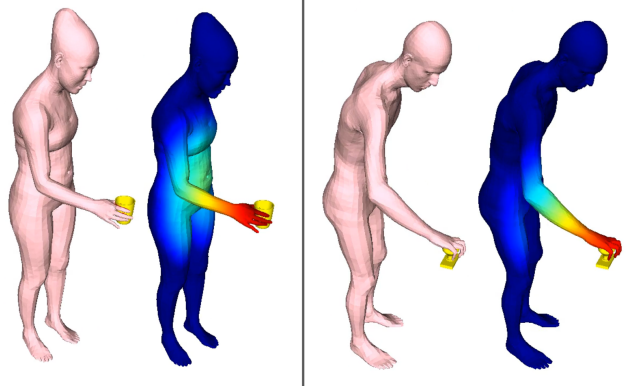


Figure 4. Visualization of the “interaction-aware” attention for body-to-object vertex distances ([Sec. 3.2](#)). For each frame the figure shows: **(Left)** Input 3D meshes for the human (pink) and the object (yellow). **(Right)** The color-coded body mesh to show our interaction-aware attention; blue denotes body vertices that are far from the object (i.e., irrelevant for the specific interaction), and red denotes vertices that are near the object (i.e., very relevant).

Pose and translation coupling discourages deviations from the initial ones:

$$\mathbf{E}_\theta(\theta; \hat{\theta}) = \|\theta - \hat{\theta}\|_2, \quad \mathbf{E}_t(t; \hat{t}) = \|t - \hat{t}\|_1. \quad (6)$$

Similarly, head-orientation coupling is formulated as:

$$\mathbf{E}_h(\theta; t; \hat{h}) = \|\mathbf{h}(\theta; t) - \hat{h}\|_2. \quad (7)$$

Finally, we find the lowest vertex of the body along the y-axis (vertical axis) and enforce its y-coordinate to be zero to have contact and prevent penetration using:

$$\mathbf{E}_f = \mathbf{v}_{k,y}^s, \quad k = \arg \min_j \mathbf{v}_{j,y}^s. \quad (8)$$

Our final energy is a combination of the above five terms:

$$\mathbf{E} = \lambda_v \mathbf{E}_d + \lambda_t \mathbf{E}_t + \lambda_p \mathbf{E}_p + \lambda_h \mathbf{E}_h + \lambda_f \mathbf{E}_f. \quad (9)$$

The efficacy of our optimization post processing using the predicted Euclidean-space interaction features, is evaluated in the next section with a perceptual study ([Tab. 2](#)).

### 3.4. Motion Network (MNet)

MNet generates the motion from the starting to the “goal” frame; the latter is generated by GNet above. The length of a sequence depends on several factors, like the object location w.r.t. the body and the speed of motion. Therefore, to generate motion of arbitrary length, we use an auto-regressive network architecture [17, 54].

**Input:** MNet takes as input (auto-regressive fashion):

$$\mathbf{X}_p = [\Theta_{t-5:t}, \beta, \mathbf{v}_t, \dot{\mathbf{v}}_t, d_t^h, b_g^h] \quad (10)$$

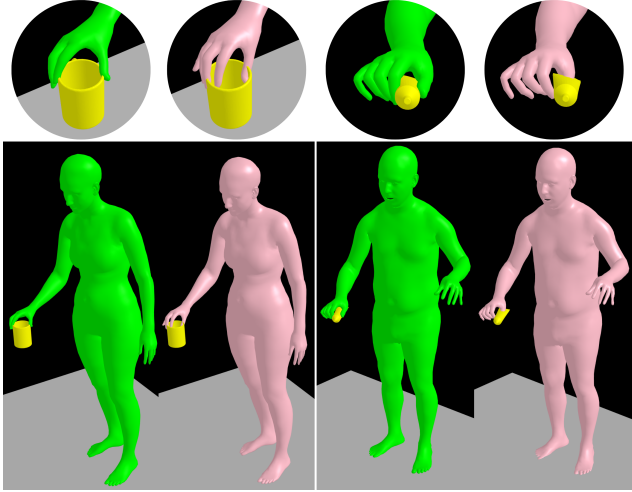


Figure 5. Generated SMPL-X grasp poses from GNet (Sec. 3.3), before (pink) and after optimization (green). Results show that optimization-based post-processing effectively refines the initial prediction towards a more realistic and physically plausible grasp.

where  $\Theta_{t-5:t}$  are SMPL-X parameters of the last 5 frames,  $\beta$  is the subject’s shape,  $v_t$  and  $\dot{v}_t$  are the locations and velocities of the sampled body vertices in the current frame,  $d_t^h$  are the hand vertex offsets from the current to the “goal” pose, and  $b_g^h$  is the BPS representation of the hand in the “goal” grasping frame. For this, we use the same BPS points as for the object. The BPS representation encodes the spatial relationship between the hand and the object in the “goal” frame, and is empirically important for “guiding” the motion towards a grasp with a good hand pose and hand-object contact. For our auto-regressive scheme, in agreement with [54], we empirically find that using more than 1 past frame leads to a smoother motion prediction; more than 5 frames do not lead to noticeable improvement.

Similar to GNet, along with predicting SMPL-X model parameters  $\Theta \in SE(3)$ , we also predict interaction features that lie in the Euclidean space. Empirically, this improves network inference, i.e. the generated motion is smoother and better “reaches” the “goal” grasp. Unlike [51], where each motion frame depends only on 1 past frame, we find that MNet’s generated motion quality improves as the number of future frames it generates grows; see Tab. 3.

**Output:** As output MNet network produces:

$$X_f = [\Delta\theta_{t+10}, \Delta t_{t+10}, \Delta v_{t+10}, \Delta d_{t+10}^h] \quad (11)$$

where  $t + 10$  denotes the future 10 motion frames,  $\Delta\theta_{t+10}, \Delta t_{t+10}$ , denote the change of SMPL-X pose and translation parameters,  $\Delta v_{t+10}$  is the change of SMPL-X vertex locations, and  $\Delta d_{t+10}^h$  is the change of hand vertex offsets. All changes,  $\Delta$ , are relative to the current frame. In an auto-regressive fashion, MNet estimates SMPL-X parameters for “motion” poses, and then these are fed back to

MNet as inputs (along with other ones) for the next iteration. For the exact architecture of MNet, see **Appx.**

MNet is trained end-to-end, with a loss similar to GNet. Specifically, we use a loss term on hand-to-object offsets, body parameters, body and hand vertices, similar to  $\mathcal{L}_d^h, \mathcal{L}_p, \mathcal{L}_v, \mathcal{L}_v^h$  in Eq. (4) respectively.

One common limitation of motion generation methods is “skating”, i.e. foot sliding on the ground. To account for this, we define an additional loss term on foot vertices, when these are close to the ground. This loss, along with the computed input velocities for Eq. (10), result in more realistic foot-ground contact; see **video** in **Appx.**

**MNet Optimization:** We refine MNet’s generated motion with post processing based on optimization; this refines the motion for better “reaching” the “goal” grasping pose generated by GNet. Since we need precision only when the hand is very close to the object, we apply the optimization step only when MNet’s estimated hand vertices get closer than 10 cm to the “goal” hand vertex positions.

We follow GNet’s scheme, and use MNet’s predictions (Eq. (11)) as constraints, instead of hand-crafted ones. We first compute the average value of MNet’s predicted hand-vertex velocities,  $\dot{v}_t^h$ . Then, we linearly interpolate between the “goal”,  $v_g^h$ , and “current”,  $v_t^h$ , hand vertices:

$$v_{t+1}^h = v_t^h + \|\dot{v}_t^h\| \times \hat{l}, \hat{l} = \frac{\vec{v}_g^h - \vec{v}_t^h}{\|\vec{v}_g^h - \vec{v}_t^h\|} \quad (12)$$

where  $\|\dot{v}_t^h\|$  is the average-velocity magnitude, and  $\hat{l}$  is the (unit) vector pointing from “current” to the “goal” hand vertices. In practice, we “force” hands to move towards the “goal” grasp in a (locally) linear trajectory. Since our focus here is the hand grasp, for the rest of the body we keep the pose and velocity that MNet predicts.

The optimization objective function  $L$  uses loss terms on hand vertices,  $\mathcal{L}_v^h$ , and on SMPL-X pose parameters,  $\mathcal{L}_p$ , similar to the ones described for Eq. (4), and has the form:

$$L = \lambda_p L_p + \lambda_h L_h. \quad (13)$$

### 3.5. Implementation Details

**Optimization details:** For both GNet’s and MNet’s optimization-based post processing, we perform gradient descent with Adam [28] to optimize SMPL-X parameters.

**Training data:** For training both GNet and MNet, we use the GRAB dataset [55], which contains whole-body 3D SMPL-X humans grasping 3D objects. Please refer to **Appx.** for the details of data preparation.

## 4. Experiments

### 4.1. Qualitative Experiments

We show examples of GNet’s generated grasp before and after optimization in Fig. 5. Results show that GNet gen-

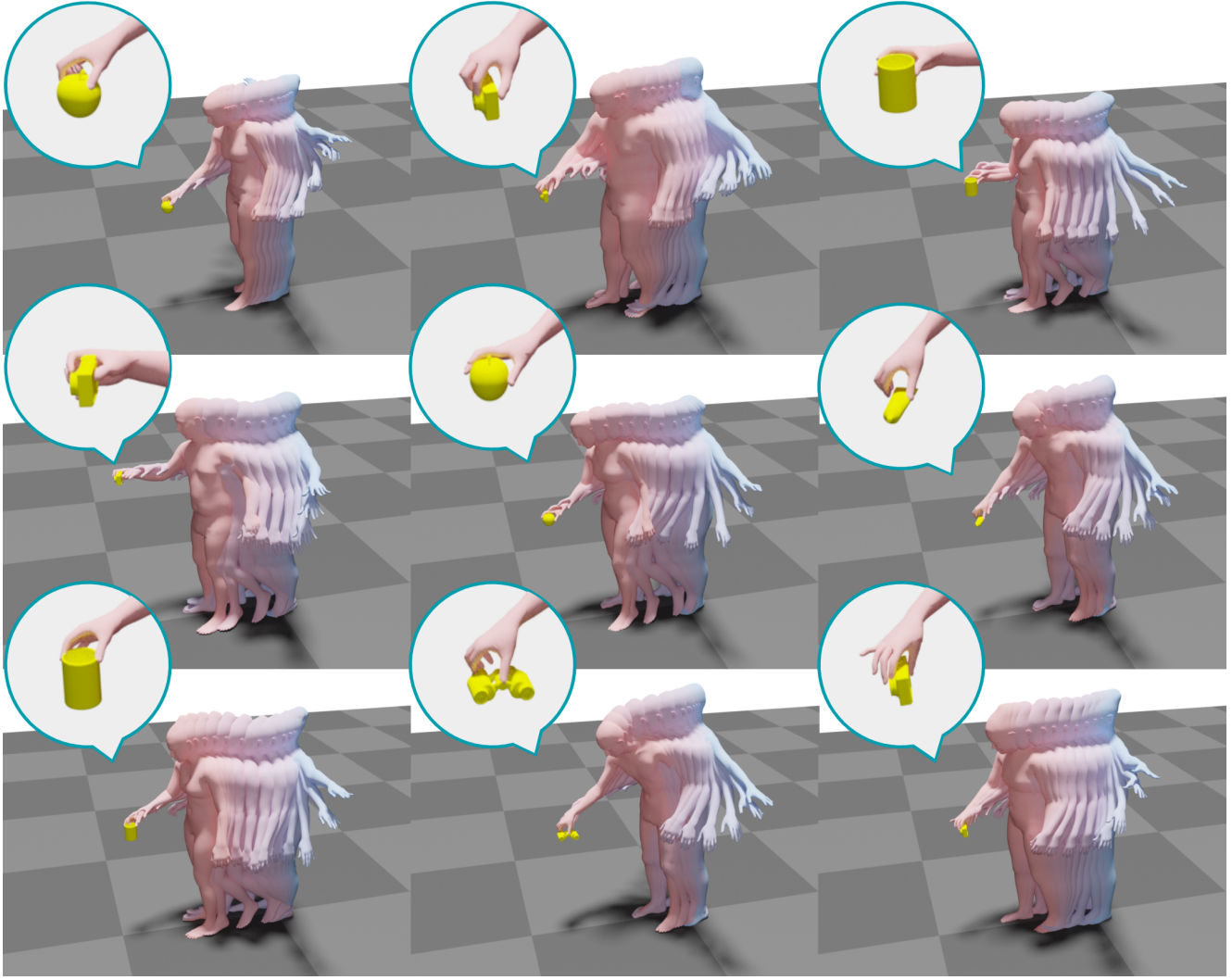


Figure 6. GOAL results: We show representative generated motions with different objects shapes, location as well as various body shapes.

erates plausible body pose and head orientation for static grasps, but the hand grasps have room for improvement. The optimization step refines hand grasps so that they are more realistic and physically plausible. We show several representative motions generated by MNet with different objects, locations as well as various body shapes in [Fig. 6](#). For more results, please see our [video](#) and [Appx](#).

#### 4.2. Quantitative Experiments

**Perceptual Study:** To quantitatively evaluate the generated results from GNet and MNet, we perform a perceptual study through Amazon Mechanic Turk (AMT).

**GNet:** For each test-set object, we use GNet to generate 2 “goal” whole-body grasps. We render a “turntable animation” of the generated grasps, before and after optimization, as well as the corresponding ground-truth grasps. Participants are asked to rate the quality of 4 features: (1) grasping

pose, (2) foot-ground contact, (3) hand-object grasp, and (4) head orientation. They rate the realism of each feature using a Likert scale of scores between 1 (unrealistic) to 5 (very realistic). Each grasp is evaluated by at least 10 participants. To remove invalid ratings, e.g., participants that do not understand the task, we use catch trials similar to GRAB [55]. The results of the evaluation are reported in [Tab. 1](#). The study shows the effectiveness of the optimization step, especially on making the hand grasps more realistic.

The study shows that the optimized grasps have a better quality in grasping pose and head orientation compared to the ground truth. This is because in a subset of the GRAB dataset the subject looks away while grasping the object, but in GNet results the head is always oriented towards the object. The higher rating in the feet-ground penetration is due to the direct loss term in our optimization process which results in a better feet-ground contact. Overall, the quality

Metric	GNet	GNet + Opt	Ground truth [55]
Overall Grasping Pose $\uparrow$	$3.89 \pm 0.93$	$3.98 \pm 0.94$	$3.78 \pm 1.06$
Foot-Ground Contact $\uparrow$	$3.98 \pm 1.06$	$4.10 \pm 0.93$	$3.82 \pm 1.11$
Hand-Object Grasp $\uparrow$	$2.70 \pm 1.37$	$3.63 \pm 1.16$	$3.98 \pm 1.04$
Head Orientation $\uparrow$	$3.83 \pm 1.01$	$4.01 \pm 0.97$	$3.84 \pm 1.07$
Average $\uparrow$	$3.60 \pm 1.22$	$3.93 \pm 1.02$	$3.86 \pm 1.07$

Table 1. Evaluation of GNet results, without and with optimization post processing. We ask the study participants to rate the realism of the grasp from 1 (unrealistic) to 5 (very realistic). We report the mean rating value  $\pm$  the standard deviation, computed across all valid study participants. Optimization post processing (“GNet + Opt”) improves all of the four studied features.

Metric	GOAL	Ground-truth [55]
Overall Body Motion $\uparrow$	$3.74 \pm 0.97$	$4.20 \pm 0.90$
Foot-Ground Contact $\uparrow$	$3.88 \pm 1.14$	$4.18 \pm 1.05$
Final Hand-Object Grasp $\uparrow$	$3.66 \pm 1.05$	$4.32 \pm 0.91$
Head Orientation $\uparrow$	$3.86 \pm 1.03$	$4.18 \pm 1.00$
Average $\uparrow$	$3.79 \pm 1.05$	$4.22 \pm 0.97$

Table 2. MNet motion generation evaluation: We ask participants to rate the generated and ground-truth motion sequences on a Likert scale of 1 (unrealistic) to 5 (very realistic). The factors considered are overall body motion realism, feet-ground contact, final hand-object grasp and head orientation.

of the generated grasps are close to the ground truth.

**MNet:** We use MNet to generate grasping motions on the test set. In a perceptual study we show participants generated sequences and ground-truth ones, and ask them to rate: (1) the overall body motion quality, (2) foot-ground contact and sliding, (3) hand-object grasp at the end of the motion, (4) and head orientation. Table 2 shows that GOAL generates realistic grasping motions, that approach the realism of ground truth. Note that MNet has a harder task than GNet, as it generates a full motion instead of a static pose. By comparing Tabs. 1 and 2, note that ground truth is rated higher for motions than for static poses and this is harder for MNet to match, though scores are not much lower.

**Foot-Sliding Metric:** We evaluate the physical plausibility of the generated motion using a “foot-sliding” metric. For each sequence, both generated and ground-truth ones, we find the closest vertex of the body to the ground and measure its velocity. We consider a frame to contain a “sliding” foot if the change in location of the selected foot vertex is higher than 1cm per frame. The percentage of “foot-sliding” frames in the ground truth and in the GOAL-generated sequences is 6.7%, and 13.7% respectively. Although there is room for improvement, empirically GNet’s motions have less sliding than existing work (on other data).

### 4.3. Ablation Study

**Number of Output Frames:** Here we study the effect of the number of output motion frames in MNet. To study

Number of output frames	V2V-Body $\downarrow$	V2V-Hand $\downarrow$	V2V-Feet $\downarrow$	Pose $\downarrow$	Trans $\downarrow$
1	14.70	10.60	17.10	3.67	5.84
2	11.40	7.75	12.4	3.77	4.29
3	10.43	6.7	11.60	4.00	4.07
5	9.66	5.58	9.40	4.00	3.42
10	<b>9.34</b>	<b>3.89</b>	<b>8.34</b>	<b>3.67</b>	<b>3.02</b>

Table 3. Comparison between several MNet architectures with different number of motion frames as output. The “v2v” notation shows the vertex-to-vertex distance error in the reconstruction loss of each network. “Hand” represents the right hand, and Pose and Trans are SMPL-X model parameters. The results clearly show the improvement of losses by increasing number of output frames.

this, we trained 5 networks with different numbers of output frames ranging from 1 to 10. We report the comparison in terms of the pose errors of the SMPL-X model, vertex-to-vertex distance for the body, feet, and hands between the generated results and the ground-truth. Results in Tab. 3 show that generating more frames in each iteration of the auto-regressive network helps generate more accurate results. Additionally, we have observed qualitatively that, for networks with a lower number of frames as output, sometimes the motion does not converge to a final grasp, and the hands gradually deviate from the object.

## 5. Conclusion and Future Work

We introduce GOAL, the first model to generate realistic human motions to grasp previously unseen 3D objects. We use two novel networks (GNet and MNet) to first generate a static “goal” grasp and then inpaint the motion between the frames. We exploit the ability of both networks to infer interaction features in Euclidean space and introduce an optimization step after each network to improve the quality of the grasps and motion based on the regressed features. The evaluation shows that our framework is able to synthesize natural and physically plausible grasping motions.

GOAL opens up many possibilities for future studies on grasping motion generation. Even though GOAL generates realistic grasping motions, it is constrained to be in a close distance to the object and can not generate motions when the body is far from the object. Future work should extend this to synthesize longer walking motions, prior to interaction with objects. In addition, in this work we focus on human-object interaction; in future work we would like to combine GOAL with human-scene interaction models to generate scene-aware grasping motions.

**Social Impact:** While realistic motion generation has mostly positive use cases in VR/AR, games, and movies, with the recent advances in neural rendering and deepfakes, we see a possibility that our results could be used for full-body deepfakes. Being aware of this, we will make our models available only for research purposes.

**Acknowledgements:** This research was partially supported by the International Max Planck Research School for Intelligent Systems (IMPRS-IS) and the Max Planck ETH Center for Learning Systems (CLS). We thank Tsvetelina Alexiadis for the Mechanical Turk experiments, and Taylor McConnell for the voice recordings.

**Disclosure:** MJB has received research gift funds from Adobe, Intel, Nvidia, Facebook, and Amazon. While MJB is a part-time employee of Amazon, his research was performed solely at, and funded solely by, Max Planck. MJB has financial interests in Amazon, Datagen Technologies, and Meshcapade GmbH.

## References

- [1] Rami Ali Al-Asqhar, Taku Komura, and Myung Geol Choi. Relationship descriptors for interactive motion adaptation. In *Symposium on Computer Animation (SCA)*, pages 45–53, 2013. [3](#)
- [2] Norman I. Badler, Cary B. Phillips, and Bonnie Lynn Webber. *Simulating Humans: Computer Graphics Animation and Control*. Oxford University Press, Inc., USA, 1993. [3](#)
- [3] Júlia Borras and Tamim Asfour. A whole-body pose taxonomy for loco-manipulation tasks. In *IEEE/RSJ International Conference on Intelligent Robots and Systems (IROS)*, pages 1578–1585, 2015. [3](#)
- [4] Matthew Brand and Aaron Hertzmann. Style machines. In *International Conference on Computer Graphics and Interactive Techniques (SIGGRAPH)*, pages 183–192, 2000. [3](#)
- [5] Yu-Wei Chao, Jimei Yang, Weifeng Chen, and Jia Deng. Learning to sit: Synthesizing human-chair interactions via hierarchical control. In *AAAI Conference on Artificial Intelligence*, pages 5887–5895, 2021. [3](#)
- [6] Tao Chen, Jie Xu, and Pulkit Agrawal. A system for general in-hand object re-orientation. *Conference on Robot Learning (CoRL)*, 2021. [3](#)
- [7] Enric Corona, Albert Pumarola, Guillem Alenyà, and Francesc Moreno-Noguer. Context-aware human motion prediction. In *Computer Vision and Pattern Recognition (CVPR)*, pages 6990–6999, 2020. [3](#)
- [8] Enric Corona, Albert Pumarola, Guillem Alenyà, Francesc Moreno-Noguer, and Gregory Rogez. GanHand: Predicting human grasp affordances in multi-object scenes. In *Computer Vision and Pattern Recognition (CVPR)*, pages 5030–5040, 2020. [5](#)
- [9] George ElKoura and Karan Singh. Handrix: Animating the human hand. In *Symposium on Computer Animation (SCA)*, pages 110–119, 2003. [3](#)
- [10] Katerina Fragkiadaki, Sergey Levine, Panna Felsen, and Jitendra Malik. Recurrent network models for human dynamics. In *International Conference on Computer Vision (ICCV)*, pages 4346–4354, 2015. [3](#)
- [11] Guillermo Garcia-Hernando, Edward Johns, and Tae-Kyun Kim. Physics-based dexterous manipulations with estimated hand poses and residual reinforcement learning. In *IEEE/RSJ International Conference on Intelligent Robots and Systems (IROS)*, pages 9561–9568, 2020. [3](#)
- [12] Michael Gleicher. Retargetting motion to new characters. In *International Conference on Computer Graphics and Interactive Techniques (SIGGRAPH)*, pages 33–42, 1998. [3](#)
- [13] Anand Gopalakrishnan, Ankur Mali, Dan Kifer, Lee Giles, and Alexander G. Ororbia. A neural temporal model for human motion prediction. In *Computer Vision and Pattern Recognition (CVPR)*, pages 12116–12125, 2019. [3](#)
- [14] Helmut Grabner, Juergen Gall, and Luc Van Gool. What makes a chair a chair? In *Computer Vision and Pattern Recognition (CVPR)*, pages 1529–1536, 2011. [3](#)
- [15] Patrick Grady, Chengcheng Tang, Christopher D. Twigg, Minh Vo, Samarth Brahmabhatt, and Charles C. Kemp. ContactOpt: Optimizing contact to improve grasps. In *Computer Vision and Pattern Recognition (CVPR)*, pages 1471–1481, 2021. [3](#)
- [16] Chuan Guo, Xinxin Zuo, Sen Wang, Shihao Zou, Qingyao Sun, Annan Deng, Minglun Gong, and Li Cheng. Action2Motion: Conditioned generation of 3D human motions. In *ACM International Conference on Multimedia (MM)*, pages 2021–2029, 2020. [3](#)
- [17] Mohamed Hassan, Duygu Ceylan, Ruben Villegas, Jun Saito, Jimei Yang, Yi Zhou, and Michael J. Black. Stochastic scene-aware motion prediction. In *International Conference on Computer Vision (ICCV)*, pages 11374–11384, 2021. [3, 5](#)
- [18] Mohamed Hassan, Partha Ghosh, Joachim Tesch, Dimitrios Tzionas, and Michael J. Black. Populating 3D scenes by learning human-scene interaction. In *Computer Vision and Pattern Recognition (CVPR)*, pages 14708–14718, 2021. [3](#)
- [19] Yana Hasson, Gürkaynak Varol, Dimitris Tzionas, Igor Kalevatykh, Michael J. Black, Ivan Laptev, and Cordelia Schmid. Learning joint reconstruction of hands and manipulated objects. In *Computer Vision and Pattern Recognition (CVPR)*, pages 11807–11816, 2019. [5](#)
- [20] Edmond S. L. Ho, Taku Komura, and Chiew-Lan Tai. Spatial relationship preserving character motion adaptation. *Transactions on Graphics (TOG)*, 29(4):33:1–33:8, 2010. [3](#)
- [21] Daniel Holden, Taku Komura, and Jun Saito. Phase-functioned neural networks for character control. *Transactions on Graphics (TOG)*, 36(4):1–13, 2017. [3](#)
- [22] Daniel Holden, Jun Saito, and Taku Komura. A deep learning framework for character motion synthesis and editing. *Transactions on Graphics (TOG)*, 35(4):138:1–138:11, 2016. [3](#)
- [23] Kaijen Hsiao and Tomas Lozano-Perez. Imitation learning of whole-body grasps. In *IEEE/RSJ International Conference on Intelligent Robots and Systems (IROS)*, pages 5657–5662, 2006. [3](#)
- [24] Changgu Kang and Sung-Hee Lee. Environment-adaptive contact poses for virtual characters. *Computer Graphics Forum (CGF)*, 33(7):1–10, 2014. [3](#)
- [25] Mubbashir Kapadia, Xu Xianghao, Maurizio Nitti, Marcelo Kallmann, Stelian Coros, Robert W. Sumner, and Markus Gross. Precision: Precomputing environment semantics for contact-rich character animation. In *Symposium on Interactive 3D Graphics (SI3D)*, 2016. [3](#)
- [26] Korrawe Karunratanakul, Jinlong Yang, Yan Zhang, Michael J. Black, Krikamol Muandet, and Siyu Tang. Grasping Field: Learning implicit representations for human

grasps. In *International Conference on 3D Vision (3DV)*, pages 333–344, 2020. 3

[27] Vladimir G Kim, Siddhartha Chaudhuri, Leonidas Guibas, and Thomas Funkhouser. Shape2pose: Human-centric shape analysis. *Transactions on Graphics (TOG)*, 33(4):120:1–120:12, 2014. 3

[28] Diederik P. Kingma and Jimmy Ba. Adam: A method for stochastic optimization. In *International Conference on Learning Representations (ICLR)*, 2015. 6

[29] Diederik P. Kingma and Max Welling. Auto-encoding variational bayes. In *International Conference on Learning Representations (ICLR)*, 2014. 4, 5

[30] Paul G. Kry and Dinesh K. Pai. Interaction capture and synthesis. *Transactions on Graphics (TOG)*, 25(3):872–880, 2006. 3

[31] Jehee Lee, Jinxiang Chai, Paul S. A. Reitsma, Jessica K. Hodgins, and Nancy S. Pollard. Interactive control of avatars animated with human motion data. *Transactions on Graphics (TOG)*, 21(3):491–500, 2002. 3

[32] Kang Hoon Lee, Myung Geol Choi, and Jehee Lee. Motion patches: Building blocks for virtual environments annotated with motion data. *Transactions on Graphics (TOG)*, 25(3):898–906, 2006. 3

[33] Kurt Leimer, Andreas Winkler, Stefan Ohrhallinger, and Przemyslaw Musalski. Pose to seat: Automated design of body-supporting surfaces. *Computer Aided Geometric Design (CAGD)*, 79, 2020. 3

[34] Ruilong Li, Shan Yang, David A. Ross, and Angjoo Kanazawa. AI Choreographer: Music conditioned 3D dance generation with AIST++. In *International Conference on Computer Vision (ICCV)*, pages 13401–13412, 2021. 3

[35] Juncong Lin, Takeo Igarashi, Jun Mitani, Minghong Liao, and Ying He. A sketching interface for sitting pose design in the virtual environment. *Transactions on Visualization and Computer Graphics (TVCG)*, 18(11):1979–1991, 2012. 3

[36] Matthew Loper, Naureen Mahmood, and Michael J. Black. MoSh: Motion and shape capture from sparse markers. *Transactions on Graphics (TOG)*, 33(6):220:1–220:13, 2014. 2, 5

[37] Matthew Loper, Naureen Mahmood, Javier Romero, Gerard Pons-Moll, and Michael J. Black. SMPL: A Skinned Multi-Person Linear Model. *Transactions on Graphics (TOG)*, 34(6):248:1–248:16, 2015. 3

[38] Christian Mandery, Ömer Terlemez, Martin Do, Nikolaus Vahrenkamp, and Tamim Asfour. The KIT whole-body human motion database. In *International Conference on Advanced Robotics (ICAR)*, pages 329–336, 2015. 3

[39] Wei Mao, Miaomiao Liu, and Mathieu Salzmann. History repeats itself: Human motion prediction via motion attention. In *European Conference on Computer Vision (ECCV)*, volume 12359, pages 474–489, 2020. 3

[40] Wei Mao, Miaomiao Liu, Mathieu Salzmann, and Hongdong Li. Learning trajectory dependencies for human motion prediction. In *International Conference on Computer Vision (ICCV)*, pages 9488–9496, 2019. 3

[41] Julieta Martinez, Michael J. Black, and Javier Romero. On human motion prediction using recurrent neural networks. In *Computer Vision and Pattern Recognition (CVPR)*, pages 4674–4683, 2017. 3

[42] Julieta Martinez, Rayat Hossain, Javier Romero, and James J. Little. A simple yet effective baseline for 3D human pose estimation. In *International Conference on Computer Vision (ICCV)*, pages 2659–2668, 2017. 3

[43] Josh Merel, Saran Tunyasuvunakool, Arun Ahuja, Yuval Tassa, Leonard Hasenclever, Vu Pham, Tom Erez, Greg Wayne, and Nicolas Heess. Catch & Carry: Reusable neural controllers for vision-guided whole-body tasks. *Transactions on Graphics (TOG)*, 39(4):39, 2020. 3

[44] Georgios Pavlakos, Vasileios Choutas, Nima Ghorbani, Timo Bolkart, Ahmed A. A. Osman, Dimitrios Tzionas, and Michael J. Black. Expressive body capture: 3D hands, face, and body from a single image. In *Computer Vision and Pattern Recognition (CVPR)*, pages 10975–10985, 2019. 2, 3, 4

[45] Xue Bin Peng, Pieter Abbeel, Sergey Levine, and Michiel van de Panne. DeepMimic: Example-guided deep reinforcement learning of physics-based character skills. *Transactions on Graphics (TOG)*, 37(4):143:1–143:14, 2018. 3

[46] Xue Bin Peng, Glen Berseth, and Michiel Van de Panne. Terrain-adaptive locomotion skills using deep reinforcement learning. *Transactions on Graphics (TOG)*, 35(4):81:1–81:12, 2016. 3

[47] Mathis Petrovich, Michael J. Black, and Gülcin Varol. Action-conditioned 3D human motion synthesis with transformer VAE. In *International Conference on Computer Vision (ICCV)*, pages 10985–10995, 2021. 3

[48] Sören Pirk, Vojtech Krs, Kaimo Hu, Suren Deepak Rajasekaran, Hao Kang, Yusuke Yoshiyasu, Bedrich Benes, and Leonidas J. Guibas. Understanding and exploiting object interaction landscapes. *Transactions on Graphics (TOG)*, 36(3):31:1–31:14, 2017. 3

[49] Nancy S. Pollard and Victor Brian Zordan. Physically based grasping control from example. In *International Conference on Computer Graphics and Interactive Techniques (SIGGRAPH)*, pages 311–318, 2005. 3

[50] Sergey Prokudin, Christoph Lassner, and Javier Romero. Efficient learning on point clouds with basis point sets. In *Computer Vision and Pattern Recognition (CVPR)*, pages 4331–4340, 2019. 4

[51] Davis Rempe, Tolga Birdal, Aaron Hertzmann, Jimei Yang, Srinath Sridhar, and Leonidas J. Guibas. HuMoR: 3D human motion model for robust pose estimation. In *International Conference on Computer Vision (ICCV)*, pages 11488–11499, 2021. 6

[52] Kathleen M. Robinette, Sherri Blackwell, Hein Daanen, Mark Boehmer, Scott Fleming, Tina Brill, David Hoeferlin, and Dennis Burnsides. Civilian American and European Surface Anthropometry Resource (CAESAR) final report. Technical Report AFRL-HE-WP-TR-2002-0169, US Air Force Research Laboratory, 2002. 4

[53] Javier Romero, Dimitrios Tzionas, and Michael J. Black. Embodied hands: Modeling and capturing hands and bodies together. *Transactions on Graphics (TOG)*, 36(6):245:1–245:17, 2017. 3

[54] Sebastian Starke, He Zhang, Taku Komura, and Jun Saito. Neural state machine for character-scene interactions. *Transactions on Graphics (TOG)*, 38(6):209:1–209:14, 2019. 3, 5, 6, 12

[55] Omid Taheri, Nima Ghorbani, Michael J. Black, and Dimitrios Tzionas. GRAB: A dataset of whole-body human grasping of objects. In *European Conference on Computer Vision (ECCV)*, volume 12349, pages 581–600, 2020. 2, 3, 4, 6, 7, 8, 12

[56] Yongyi Tang, Lin Ma, Wei Liu, and Wei-Shi Zheng. Long-term human motion prediction by modeling motion context and enhancing motion dynamics. In *International Joint Conference on Artificial Intelligence (IJCAI)*, pages 935–941, 2018. 3

[57] Ashish Vaswani, Noam Shazeer, Niki Parmar, Jakob Uszkoreit, Llion Jones, Aidan N. Gomez, Łukasz Kaiser, and Illia Polosukhin. Attention is all you need. In *Conference on Neural Information Processing Systems (NeurIPS)*, pages 5998–6008, 2017. 3

[58] Jiashun Wang, Huazhe Xu, Jingwei Xu, Sifei Liu, and Xiaolong Wang. Synthesizing long-term 3D human motion and interaction in 3D scenes. In *Computer Vision and Pattern Recognition (CVPR)*, pages 9401–9411, 2021. 3, 5

[59] Jack M. Wang, David J. Fleet, and Aaron Hertzmann. Gaussian process dynamical models for human motion. *Transactions on Pattern Analysis and Machine Intelligence (TPAMI)*, 30(2):283–298, 2008. 3

[60] Yuting Ye and Karen C. Liu. Synthesis of detailed hand manipulations using contact sampling. *Transactions on Graphics (TOG)*, 31(4):41:1–41:10, 2012. 3

[61] Ye Yuan and Kris Kitani. DLow: Diversifying latent flows for diverse human motion prediction. In *European Conference on Computer Vision (ECCV)*, volume 12354, pages 346–364, 2020. 3

[62] Mihai Zanfir, Andrei Zanfir, Eduard Gabriel Bazavan, William T. Freeman, Rahul Sukthankar, and Cristian Sminchisescu. THUNDR: Transformer-based 3D human reconstruction with markers. In *International Conference on Computer Vision (ICCV)*, pages 12971–12980, 2021. 2, 5

[63] Siwei Zhang, Yan Zhang, Qianli Ma, Michael J. Black, and Siyu Tang. PLACE: Proximity learning of articulation and contact in 3D environments. In *International Conference on 3D Vision (3DV)*, pages 642–651, 2020. 3

[64] Yan Zhang, Michael J. Black, and Siyu Tang. We are more than our joints: Predicting how 3D bodies move. In *Computer Vision and Pattern Recognition (CVPR)*, pages 3372–3382, 2021. 2, 3, 5

[65] Yan Zhang, Mohamed Hassan, Heiko Neumann, Michael J. Black, and Siyu Tang. Generating 3D people in scenes without people. In *Computer Vision and Pattern Recognition (CVPR)*, pages 6193–6203, 2020. 3

[66] Youyi Zheng, Han Liu, Julie Dorsey, and Niloy J Mitra. Ergonomics-inspired reshaping and exploration of collections of models. *Transactions on Visualization and Computer Graphics (TVCG)*, 22(6):1732–1744, 2015. 3

[67] Yi Zhou, Connelly Barnes, Jingwan Lu, Jimei Yang, and Hao Li. On the continuity of rotation representations in neural networks. In *Computer Vision and Pattern Recognition (CVPR)*, pages 5745–5753, 2019. 4

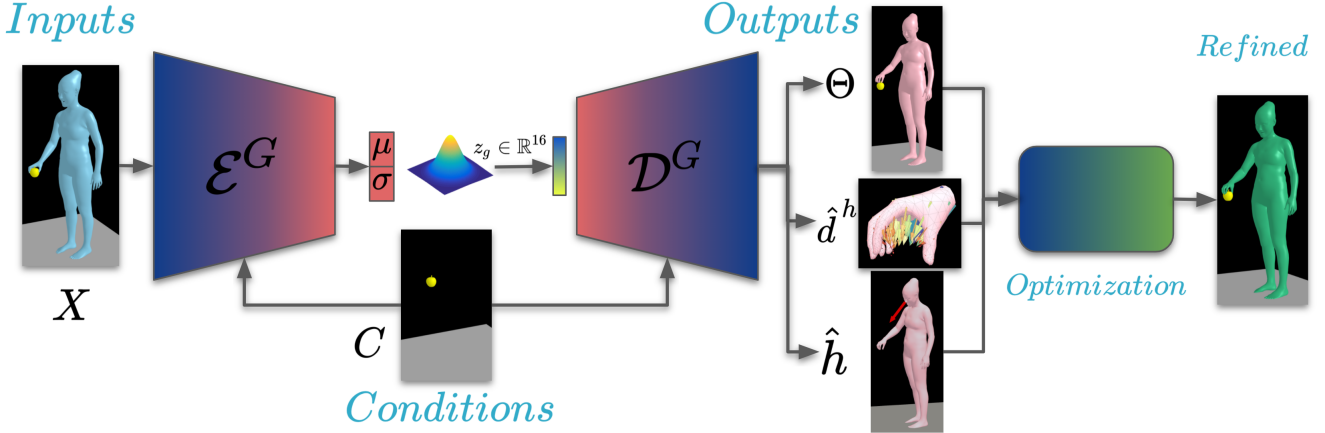


Figure A.7. Architectural overview of the GNet network, as well as of the optimization post-processing step (right-most part).

## Appendix

### A.1 Data Preparation

**GNet data preparation:** GNet generates static grasps. Therefore, we collect from the GRAB [55] dataset all frames with right-hand grasps (without loss of generality), for which participants grasp the object in a stable way. For this, we follow the selection criteria used for GrabNet's [55] training data. We then center the object at the origin along the horizontal plane, i.e., while preserving its height. In total, we collect 160K, 26K, and 12.5K frames for the training, testing, and validation set, respectively.

**MNet data preparation:** MNet generates motion. Thus, we gather from each sequence of GRAB all frames from the starting one up to the frame where the right hand (without loss of generality) first establishes a stable grasp. For this, we use the same selection criteria as above for GNet. We then create several sub-sequences by sliding a 21-frame window over each sequence with a stride of 1 frame. For each sub-sequence, we consider the first 10 frames as “past” motion, the last 10 frames as “future” motion, and the middle one as the “current” frame. Then, following [54], we make all “past” and “future” frames relative to the body coordinate system of the “current” frame, while keeping the gravity direction always upward. In total, we collect roughly 40K, 7K, and 3K motion sub-sequences for the training, testing, and validation sets, respectively.

### A.2 GNet Architecture

For an architectural overview of GNet and its optimization-based post processing, see Fig. A.7. During training, the encoder  $E^G$  maps the inputs  $X$  to the parameters of a normal distribution  $\mu, \sigma \in \mathbb{R}^{16}$ . We then sample a latent whole-body grasp code  $z_g \in \mathbb{R}^{16}$  from this distribution, concatenate it with the object BPS representation and object height, and then pass it to the decoder  $D^G$ . The decoder outputs the SMPL-X parameters  $\Theta$ , the head direction vector  $\hat{h}$ , and hand-to-object offset vectors  $\hat{d}^h$ . Finally, we use the predicted offsets and head orientation to refine GNet's SMPL-X predictions with an optimization step.

ters of a normal distribution  $\mu, \sigma \in \mathbb{R}^{16}$ . We then sample a latent whole-body grasp code  $z_g \in \mathbb{R}^{16}$  from this distribution, concatenate it with the object BPS representation and object height, and then pass it to the decoder  $D^G$ . The decoder outputs the SMPL-X parameters  $\Theta$ , the head direction vector  $\hat{h}$ , and hand-to-object offset vectors  $\hat{d}^h$ . Finally, we use the predicted offsets and head orientation to refine GNet's SMPL-X predictions with an optimization step.

### A.3 MNet Architecture

For an architectural overview of MNet and its optimization-based post processing, see Fig. A.8. MNet is an auto-regressive network and in each iteration it takes as input the features of the last 5 frames and GNet's “goal” frame. As output it gives the change in SMPL-X model parameters ( $\Delta\Theta_{t+10}$ ), the change of SMPL-X vertex locations ( $\Delta v_{t+10}$ ), and the change of hand vertex offsets ( $\Delta d_{t+10}^h$ ) for the future 10 frames. In the beginning of motion generation, where we only have the “start” motion frame and no past frame, the “start” frame is repeated 5 times. Note that, due to its auto-regressive fashion, GOAL is not constrained to a specific “start” body pose and generalizes well to any pose, i.e. articulation (with a distance and orientation w.r.t. the object in a reasonable range).

### A.4 Video

We provide a narrated video that: (1) explains our motivation, (2) explains our method, and (3) shows many results, including qualitative motions. This is important, as motion realism is better evaluated with a video; please see it at <https://goal.is.tuebingen.mpg.de>.

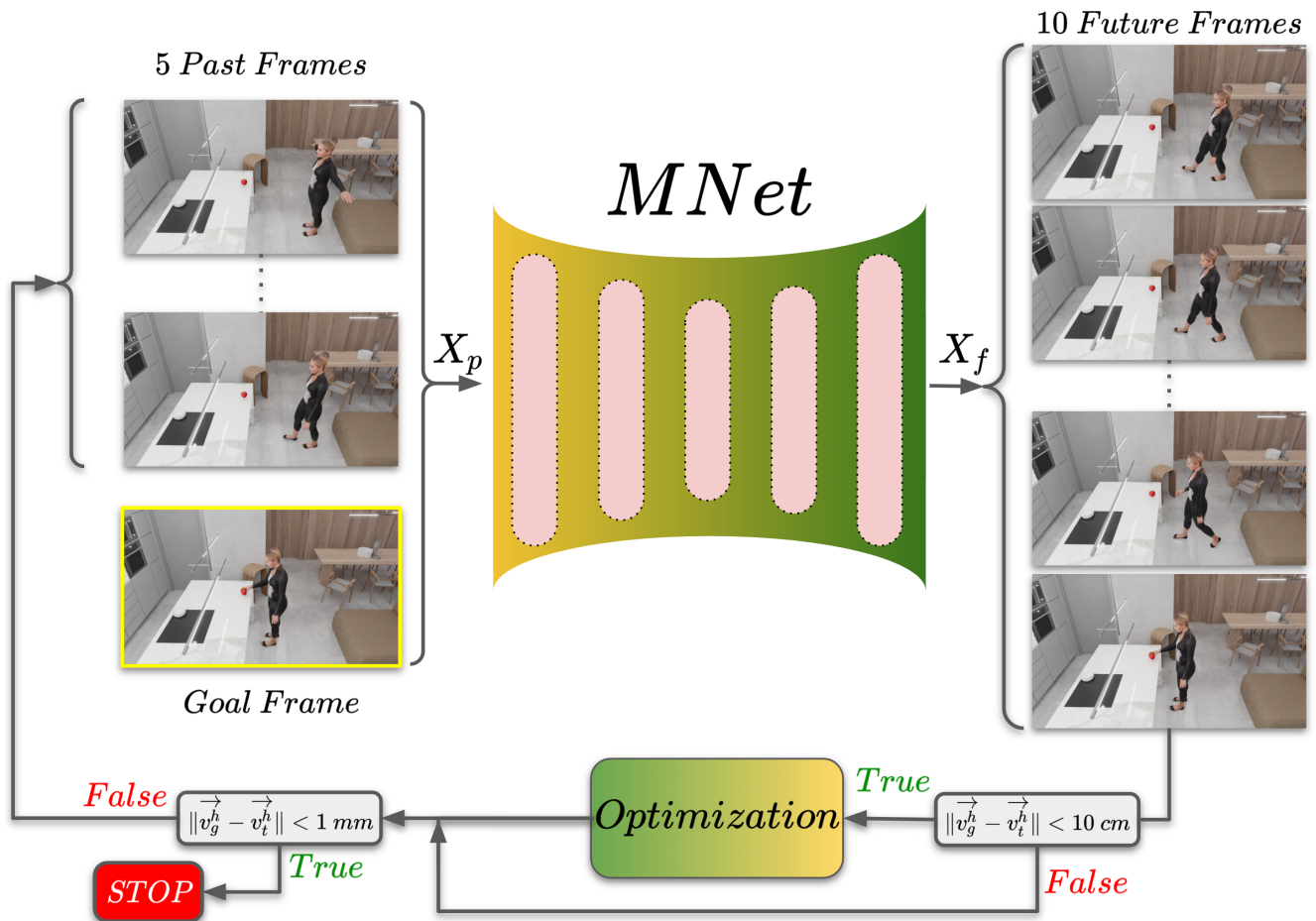


Figure A.8. Architectural overview of the MNet network, as well as of the optimization post-processing step (bottom part).